A Wrist for Needle-Sized Surgical Robots

Peter A. York, *Student Member, IEEE*, Philip J. Swaney, *Student Member, IEEE*,
Hunter B. Gilbert, *Student Member, IEEE*, and Robert J. Webster III, *Senior Member, IEEE*

Abstract— The needle-sized surgical tools used in arthroscopy, otolaryngology, and other surgical fields could become even more valuable to surgeons if endowed with the ability to navigate around sharp corners to manipulate or visualize tissue. We present a needle-sized wrist design that grants this ability. It can be easily interfaced with manual tools or concentric tube robots and is straightforward and inexpensive to manufacture. The wrist consists of a nitinol tube with several asymmetric cutouts, actuated by a tendon. Perhaps counter-intuitively, within this seemingly simple design concept, design optimization is challenging due to the number of parameters available and nonlinearities in material properties. In this paper, we examine a subset of possible geometries and derive kinematic and static models. Experimental results with a 1.16 mm diameter prototype validate the models. Lastly, we provide a discussion summarizing the lessons learned in our early experience designing and fabricating wrists of this type.

I. INTRODUCTION

There is a pressing need for small-diameter wristed surgical tools. Most existing needle-sized surgical devices do not include wrists and thus cannot navigate the sharp corners encountered in surgery, such as those at the skull base [1], in the middle ear [2], and in the ankle [3]. Moreover, dexterity-driven tasks, such as tissue resection and suturing, can be difficult to perform without a wrist, especially through the small openings characteristic of natural orifice or percutaneous procedures.

In particular, needle-sized wrists are needed to augment the capabilities of concentric tube surgical robots, as noted in [4]. The performance of concentric tube robotic systems devised for pituitary tumor resection [5], neurosurgery [6], [7], and intracardiac surgery [8], among others, could potentially be significantly enhanced with the addition of wristed end-effectors.

Many small wrists based on traditional mechanical linkages have been devised in the past, including wrists with ball joints [9], [10], universal joints [11], cables and pulleys [12], [13], [14], [15], lead screws [16], [17], serial chains in parallel [18], and flexures [19], [20], [21]. These designs range from 2.4 to 15 mm. Although it is undoubtedly

Fig. 1: Photograph of a wrist mounted to the tip of a concentric tube robot. The diameter of the wrist is 1.16 mm.

possible to downscale each of these designs to some degree, designs with a continuum structure are typically easier to miniaturize than those containing multiple components. A variety of continuum wrists have been devised, including those of Breedveld et al. [22], Herder et al. [23], Peirs et al. [24], and Simaan [25], among others. Among these, those with the fewest components are desirable for downscalability, making designs that involve machining the shaft of the robot itself particularly appealing.

Several groups have used the idea of cutting nitinol tube to create a compliant region for bending. Fischer et al. devised a 10-mm tool for endoscopic camera steering [26]. Kutzer et al. created a 6-mm tendon-driven tool for arthroscopy using rectangular cutouts [27]. Wei et al. created a similar manipulator using triangular cuts [28]. Several groups have recently explored methods of conducting finite element analyses to aid in design [29], [30], [31]. Our wrist design most closely resembles the catheter designs of Haga et al. and Bell et al. [32], [33] and the needle design of Ryu et al. [34]. We build on this body of work by providing kinematics and statics models and by describing a simple manufacturing process for making such cutout wrists.

We use an asymmetric cutout geometry, as shown in Fig. 2. The most significant advantage of using asymmetric cutouts is the longer moment arm between the tendon anchor point and the neutral bending plane, which enables significantly lower tendon actuation forces for devices of comparable diameter. Another significant advantage is the ability to achieve a tighter radius of curvature, since the radius of curvature is measured about the center of the wrist, whereas the wrist bends about an offset neutral bending plane. Other advantages of the asymmetric geometry include single wire actuation and simplified tendon routing, since the tendon will naturally conform to the inside wall of the tube when pulled, and one need not design mechanisms to hold it in place (e.g. the use of two nitinol tubes with the tendon
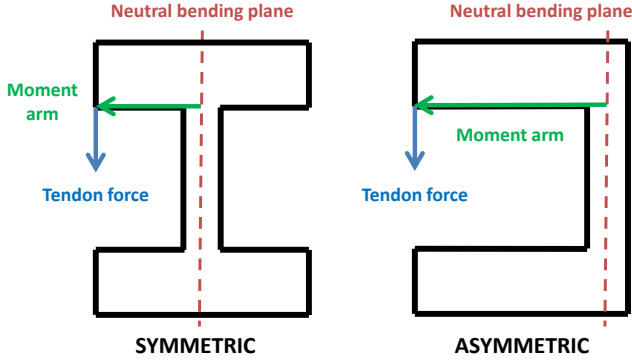
Fig. 2: Symmetric (left) vs. asymmetric (right) cutouts shown. Asymmetric cutout has much longer moment arm for the tendon force.

Fig. 3: Arc parameters and relevant kinematic values for single cutout.

sandwiched between in [27]). One potential drawback of an asymmetric wrist is that it can bend in only one direction in the plane, rather than two. However, provided axial rotation of the entire device is possible (which it typically is for such devices), the impact of this potential drawback is minimized. The potentially more significant downside of an asymmetric wrist is that while it can readily apply pulling forces, it can only apply pushing forces if the tissue being pushed is more compliant than the wrist itself. Note that it may be possible to stiffen the wrist to assist with pushing by inserting a wire through the central lumen, although we have not yet experimented with this.

In addition to being able to be manufactured and assembled at small diameters, the continuum cutout design also offers a large design space. Here, we restrict the problem to one of analyzing rectangular cutouts because they are straightforward to machine with a standard end mill (see Section IV). With this restriction, the design parameters available are the height, depth, and spacing between cuts, as well as the number of cuts. We present models and design principles that allow the designer to use these parameters to select the device's overall radius of curvature, total maximum bend angle, and required tendon force for actuation.

II. KINEMATICS

We begin by modeling the kinematics of a single cutout of the asymmetric continuum wrist. We assume that the portion of the tube that undergoes bending deforms in a constant curvature arc. This is a good assumption for small cut heights h, because the tendon follows an approximately circular path in this case. Following [35], we map tendon displacement (actuator space) to arc parameters (configuration space) then map arc parameters to task space. The arc parameters we seek are curvature (κ) and arc length (s), as shown in Fig. 3. The actuator space to configuration space mapping is largely dependent on the location $\bar{y}$ of the neutral bending plane. The neutral bending plane experiences no strain in bending and intersects the centroids of the axial cross sections of the cut portions of the tube. Its location is dependent on the depth of cut g and the inner and outer radii of the tube (r_i and r_o
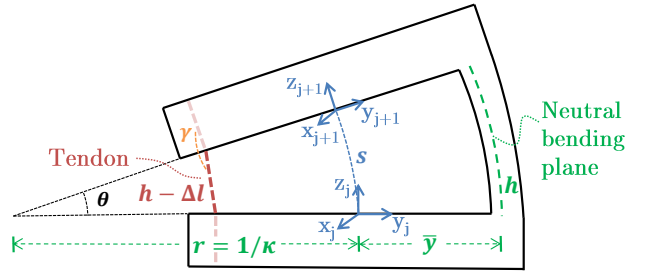
shown in Fig. 4) and is given by:

$$\bar{y} = \frac{\bar{y}_o A_o - \bar{y}_i A_i}{A_o - A_i} \quad (1)$$

where A_o and A_i are the areas defined in Figure 4 and $\bar{y}_o$ and $\bar{y}_i$ are their respective centroids. They are given by:

$$\bar{y}_o = \frac{4r_o \sin^3(\frac{1}{2}\phi_o)}{3(\phi_o - \sin\phi_o)} \qquad \bar{y}_i = \frac{4r_i \sin^3(\frac{1}{2}\phi_i)}{3(\phi_i - \sin\phi_i)}$$

$$A_o = \frac{r_o^2(\phi_o - \sin(\phi_o))}{2} \qquad A_i = \frac{r_i^2(\phi_i - \sin(\phi_i))}{2}$$

$$\phi_o = 2\arccos((g - r_o)/r_o) \quad \phi_i = 2\arccos((g - r_o)/r_i)$$
$$(2)$$

which are valid for cuts that are at least as deep as the outer radius of the tube.
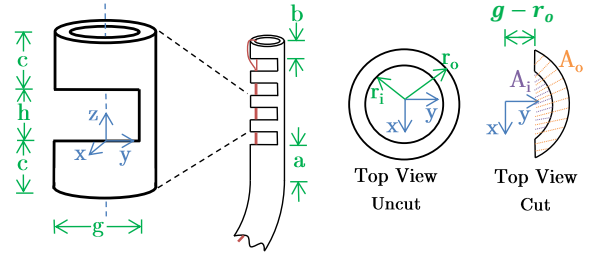

Fig. 4: The geometric parameters that the designer is free to choose are shown in green. The tendon is shown in red, looped through the top cutout. The regions of the uncut portion of the tube used for the calculation of the neutral bending plane location are shown in purple and orange.

Now we can use $\bar{y}$ to find the mapping from curvature to tendon displacement (Δl), noting Fig. 3 and using the chord function and arc geometry:

$$\Delta l = h - 2\left(\frac{1}{\kappa} - r_i\right)\sin\left(\frac{\kappa h}{2(1 + \bar{y}\kappa)}\right) \quad (3)$$

Since we want the mapping of tendon displacement to curvature, we need to invert (3). Since it has no analytic inverse, numerical techniques can be used, or, for small angles, we can use a first-order approximation to yield:

$$\kappa \approx \frac{\Delta l}{h(r_i + \bar{y}) - \Delta l\,\bar{y}} \quad (4)$$

Once κ is known, s can be found using:

$$s = \frac{h}{1 + \bar{y}\kappa} \quad (5)$$

Once the arc parameters κ and s are known, the homogeneous transformation between frames j and $j+1$ (as defined in Fig. 3) can be found using:

$$T_j^{j+1} = \begin{bmatrix} 1 & 0 & 0 & 0 \\ 0 & \cos(\kappa s) & -\sin(\kappa s) & (\cos(\kappa s) - 1)/\kappa \\ 0 & \sin(\kappa s) & \cos(\kappa s) & \sin(\kappa s)/\kappa \\ 0 & 0 & 0 & 1 \end{bmatrix} \quad (6)$$

Due to the rectangular cutout geometry of the wrist, the kinematic transformation from the base of the wrist to the tip can be obtained. The kinematics of the entire wrist are given by repeatedly applying the transformation (6) in conjunction with translations to account for the portions of the wrist that do not bend:

$$T_o^t = T_{z,a} \left(\prod_{j=1}^{n} T_j^{j+1} T_{z,c} \right) T_{z,b-c} \quad (7)$$

where n is the number of cutouts and $T_{z,a}$, $T_{z,b-c}$, and $T_{z,c}$ are translations along the z-axis by a, $b - c$, and c, respectively, as defined in Fig. 4. In addition, the angle of rotation of each section can be found explicitly as:

$$\theta_j(\kappa) = s\kappa = \left(\frac{h}{1 + \bar{y}\kappa} \right) \kappa \quad (8)$$

And thus the maximum angle of rotation for a single cutout is given by:

$$\theta_{j,max} = \theta_j(1/r_o) = \frac{h}{r_o + \bar{y}} \quad (9)$$

Two important wrist characteristics, maximum bending angle and minimum radius of curvature, as shown in Fig. 5, can be calculated from geometry as:

$$\theta_{max} = \sum_{j=0}^{n} \theta_{j,max} = n \frac{h}{r_o + \bar{y}} \quad (10)$$

$$\rho_{min} \approx r_o + \frac{(n-1)c}{\theta_{max}} \quad (11)$$

where the approximately circular arc that defines ρ_{min} has length:

$$S = n \left(\frac{r_o h}{r_o + \bar{y}} + c \right) - c \quad (12)$$

The wrist kinematics are experimentally validated in Section IV.

III. STATICS

Modeling the static behavior of the wrist is more challenging than modeling the kinematic behavior, yet with the assumption of constant curvature bending, it is tractable. Based on the constant curvature assumption, strain along the length of the wrist varies in a cross section of the portion of the tube in bending according to:

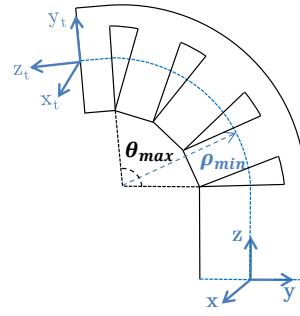$$\epsilon(y, \kappa) = \frac{\kappa(y - \bar{y})}{1 + \bar{y}\kappa} \quad (13)$$

Fig. 5: Wrist schematic with kinematic frames and minimum radius of curvature labeled.

and thus is linearly distributed about the neutral bending plane. This assumed relationship between the geometry and the material deformation allows for a simple computation of the strain energy, after which we use Castigliano's first theorem to determine the reaction force at the tendon. In general, the behavior of nitinol under applied stresses is complex and highly nonlinear, and depends on thermomechanical history [36]. In this work we assume a simplified material model that represents the stress-strain behavior of nitinol as a piecewise linear stress-strain curve, so that the stress may be written as a function of strain as:

$$\sigma(\epsilon) = \begin{cases} \sigma_{lp} & \epsilon < \sigma_{lp}/E \\ E\epsilon & \sigma_{lp}/E \leq \epsilon \leq \sigma_{up}/E \\ \sigma_{up} & \epsilon > \sigma_{up}/E \end{cases} \quad (14)$$

where σ_{lp} is the lower plateau stress (corresponding to compression), σ_{up} is the upper plateau stress (corresponding to tension), and E is Young's modulus. Since we are modeling the material deformation as a one-dimensional stretching and compression of axial fibers, the strain energy density is the area under the stress-strain curve, given by the integral:

$$W(\epsilon) = \int_0^{\epsilon} \sigma(e) \, de \quad (15)$$

The total strain energy stored in the wrist as a function of the curvature κ of a single cutout is given by:

$$U(\kappa) = n \int_{V_c} W(\epsilon(y, \kappa)) \, dV \quad (16)$$

where V_c is the volume defined by the "Top View Cut" cross section of Fig. 4 and cutout height h. We use Castigliano's first theorem to find the relationship between rotation θ of the wrist and force F applied by the tendon to the wrist tip:

$$\frac{\partial U(\kappa)}{\partial \theta} = M = FL \quad (17)$$

where L is the moment arm length and $\theta = ns\kappa$. When the tendon is looped around the top flexure as shown in Fig. 4, the moment arm has length $L = \left(\frac{r_o + r_i}{2} \right) + \bar{y}$.

Due to friction, the force the tendon applies to the tip of the wrist will be a fraction of the actuator force applied to the tendon. Friction between the tendon and the tube wall becomes increasingly significant as cut height and angle of bending increase. To model this effect, we first find the angle γ (shown in Fig. 3) that the tendon is required to navigate

at a single corner of a cutout section at a given angle of deflection. We assume that the friction that occurs at these corners dominates friction elsewhere along the tendon path. Writing the static balance equations for a single corner, with μ_s as the static friction coefficient, we find that:

$$F = \eta F_{\text{tendon}} = \frac{\sin(\gamma/2) - \mu_s \cos(\gamma/2)}{\sin(\gamma/2) + \mu_s \cos(\gamma/2)} F_{\text{tendon}} \quad (18)$$

where $\eta < 1$ accounts for the force lost due to friction at a corner. We can substitute (18) into (17) to yield:

$$F_{\text{tendon}} = \frac{1}{\eta^{2n} L} \frac{\partial U(\kappa)}{\partial \theta} \quad (19)$$

where $2n$ is included to account for the two corners of each cutout. This expression can be evaluated numerically using a finite difference method to relate F_{tendon} and θ. This statics model is experimentally validated in Section IV.
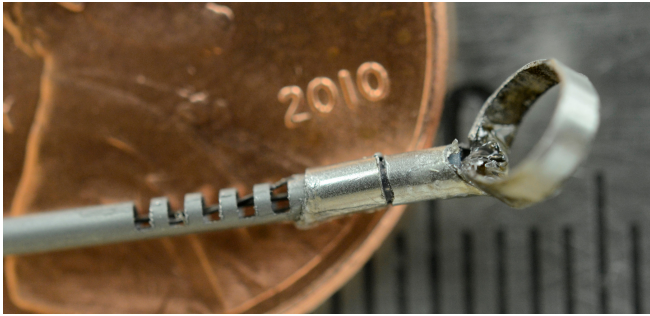
Fig. 6: A 1.16 mm diameter prototype wrist is shown with metric scale and curette. A curette is a common surgical instrument used for tissue resection. This curette is attached to a nitinol wire running through the tube and can be axially rotated by rotating the wire.

IV. PROTOTYPE & EXPERIMENTS

Our prototype is shown in Figs. 6, 7, and 8. We used a MicroProto Systems MicroMill 2000 CNC mill (a small tabletop CNC that cost approximately $2500 to purchase new) with aluminum titanium nitride coated, two flute, carbide, long flute, 0.02" diameter square end mills to manufacture our prototypes. We fixtured the tube by gluing it in a channel drilled in an aluminum block. We used nitinol tube with outer diameter $1.16\,\text{mm}$ and inner diameter $0.86\,\text{mm}$. We chose a cut depth of $g = 0.97\,\text{mm}$ which corresponds to a required tendon force for full bending of $F_{\text{tendon}} = 5\,\text{N}$ and a maximum outer-fiber strain of 10.4% [1]. We selected a cut height of $h = 0.51\,\text{mm}$, spacing between cuts of $c = 0.51\,\text{mm}$, and $n = 5$ cuts in order to achieve greater than $90°$ of bending. A summary of the design parameter choices and resulting design characteristics is shown in Table I.

We conducted an experiment to validate the kinematic relationship (7) and static relationship (19) concurrently. Our experimental setup included a linear slide (Velmex A2512Q2-S2.5) with $0.01\,\text{mm}$ resolution to displace the tendon and a force sensor (ATI Nano 17) with $3.125\,\text{mN}$

[1] Note that this is slightly higher than the 8-10% recoverable strain typically quoted for nitinol, but that we have found it to work well in practice, since only a small amount of the material at the very outside edge of the wrist undergoes this strain, and then only at maximum articulation.

Parameter	Value		Characteristic	Value
D_o	1.16 mm		θ_{max}	138.6°
D_i	0.86 mm		ρ_{min}	1.42 mm
g	0.97 mm		ϵ_{max}	10.4%
h	0.51 mm		F_{tendon}	5 N
c	0.51 mm			
n	5			

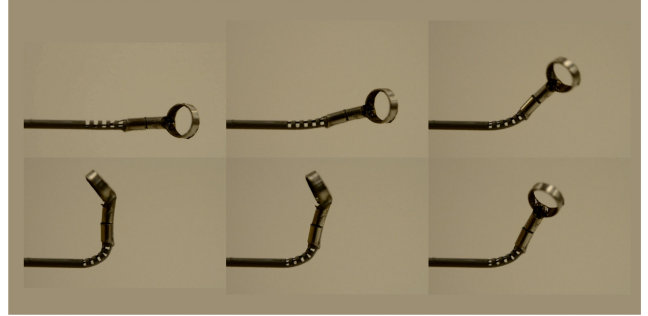TABLE I: Summary of design parameters chosen for prototype

Fig. 7: Wrist motion from 0 to 90° bending angle shown clockwise. Note that the ring curette is being rotated during the bending motion of the wrist.

resolution to record tendon force. The tendon was rigidly fixed to an acrylic plate that was then mounted onto the force sensor. The tendon and sensor assembly were then rigidly fixed to the linear slide carrier. The nitinol tube with cutout wrist was mounted into a test fixture that was rigidly mounted to an optical table, such that the tube remained stationary while the wrist was deflected with the linear slide. A 1 mm resolution grid was placed below the wrist, and a camera mounted directly above the wrist was used to capture images of the wrist as it deflected. The wrist was deflected in tendon displacements of 0.2 mm, and a picture of the wrist deflection and the tendon force were recorded at each increment. Using image processing, the tip position was determined for each incremental deflection of the tendon. We observed that at full articulation, the distal cutout was held open by the tendon that was routed through it (see Fig. 8). For this reason, the plots in Figs. 9 and 10 were made based on $n = 4$ cutouts. In future work, we plan to explore alternate tendon attachment methods to address this issue. Results are shown in Figs. 9 and 10.

Fig. 8: The prototype was experimentally validated without the curette instrument (see Fig. 6) attached. The actuation tendon held open the last cutout of the wrist during the experimental trials, and the kinematics and statics models were calculated with $n = 4$ cutouts.
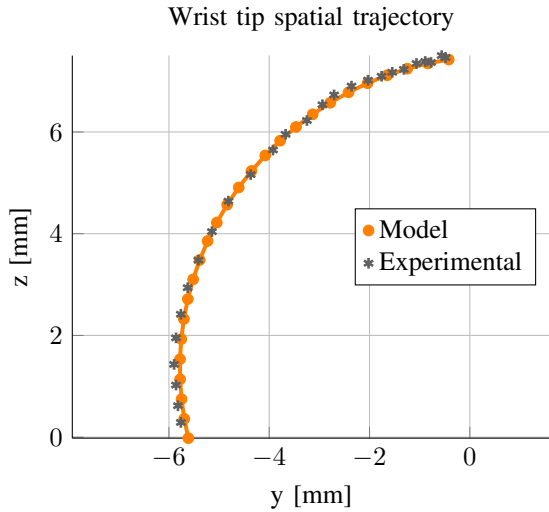
Fig. 9: The wrist starts at top of the figure and rotates counterclockwise from 0 to 110°. These results show that the constant curvature assumption is a reasonable approximation for this geometry, since the wrist tip follows the path predicted by the model.
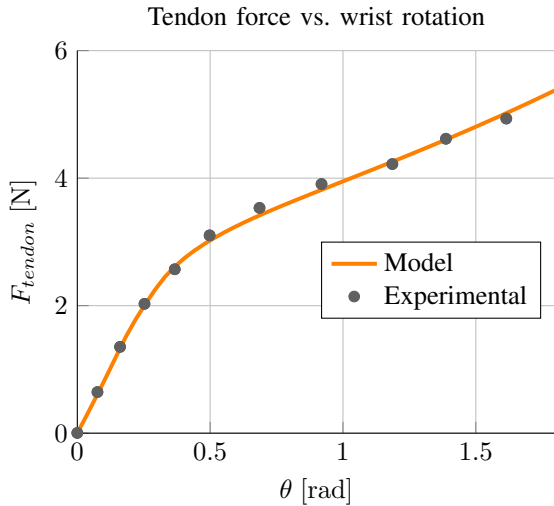

Fig. 10: The statics model is shown here with the experimental data. The model captures the superelastic behavior of the material, with the change in the slope of the graph indicating the transition of some of the volume of material into the stress plateau region.

An experimental validation of the statics model is shown in Fig. 10. For the material properties, note that nitinol has an asymmetric stress strain relationship in tension and compression. We assume plateau stresses of $\sigma_{lp} = -750\,\mathrm{MPa}$ and $\sigma_{up} = 500\,\mathrm{MPa}$ and a Young's modulus of $E = 60\,\mathrm{GPa}$, which fall within ranges reported by the manufacturer and in the literature [36], [37]. The model is shown with a coefficient of friction of 0.36, which was chosen through nonlinear least squares optimization. Note that the superelastic, nonlinear behavior of the material is clearly captured by the model.

V. DISCUSSION

The prototype we fabricated represents one set of viable design choices. With the rectangular cut profile described in previous sections, the designer must choose the depth of cut g (see Fig. 4), height of cut h, number of cuts n, and axial spacing between cuts c. Moreover, the designer also has some freedom to select the tube radii, though this is likely to be from among a finite set of options due to material availability. The tube radii and the depth of cut are the most important parameters in determining wrist behavior, because they determine the location of the neutral bending plane, which strongly affects the kinematics, strain in the bending material, and the required actuation force. A cut depth $g > r_o$ is desirable to achieve substantial bending compliance. The allowable depth of cut is bounded by the maximum allowable strain, where the maximum strain at full bending is given by:

$$\epsilon_{max} = \epsilon(r_o, 1/r_o) = \frac{r_o - \bar{y}}{r_o + \bar{y}} \qquad (20)$$

Cut height is not as significant as cut depth in determining wrist behavior, but it is a factor in the bending radius (Eq. 10 and 11). Moreover, if cut height becomes too large, the constant curvature assumption will no longer hold, risk of buckling-like failure will increase, and frictional losses will increase (Eq. 18 and 19).

The portions of uncut tube between the cutouts serve as hard stops which limit strain, allow large forces to be applied in the wrist's fully deflected state, and route the tendon in a curve that approximates a circular arc. The height of the uncut portions, parameter c in Fig. 4, should be as small as possible to minimize radius of curvature. However, as it decreases, risk of damaging the wrist during actuation and environmental interaction increases.

Additionally, if uniform curvature in multiple cutout sections is desired, it is essential to use a highly repeatable cutting process, as slightly deeper cutouts deflect much further for a given force than shallower cutouts do. That being said, it may be advantageous in future work to take advantage of non-uniform cut depths (and/or heights) to compensate for factors like non-constant tendon tension (due to frictional losses) along the wrist, or application-specific design objectives.

The experimental results show that the constant curvature assumption is a reasonable, though not perfect, approximation for our wrist. We believe that tendon elongation was the primary source of error in the kinematics, which resulted in the model and experimental tip points not aligning perfectly in Fig. 9. The coefficient of friction is likely the least well-known of all the parameters, since the amount of friction depends on factors such as surface roughness and geometry. Another potential source of error is the implicit assumption in (13) that cross sections do not deform during bending, which is a common assumption in beam bending analysis.

In the future, we plan to study the significance of hysteresis in our statics model and develop a three-dimensional stiffness model in order to characterize the forces that the wrist can exert. We also plan to conduct finite element modeling to characterize torsional properties and fatigue life and to explore strain profiles of non-rectangular cutouts. Another area of future work is to explore non-square cutout geometries to optimize wrist performance for specific tasks.

VI. Conclusion

We have presented a needle-sized, tendon-actuated cutout wrist and provided a modeling framework for it. A 1.16 mm prototype was successfully machined using a low-cost, accessible manufacturing technique and was used to validate our models. We have integrated the wrist into a concentric tube continuum robot (Fig. 1), and future work includes evaluating the wristed robot in realistic surgical scenarios including endonasal pituitary tumor removal. A wrist of the type we describe in this paper affords the designer great flexibility in optimization for task requirements. We believe this will be useful in the future in a variety of clinical applications that require dexterity in thin tools working in confined spaces.

References

[1] C. H. Snyderman, R. L. Carrau, A. B. Kassam, A. Zanation, D. Prevedello, P. Gardner, and A. Mintz, "Endoscopic skull base surgery: principles of endonasal oncological surgery," *Journal of Surgical Oncology*, vol. 97, no. 8, pp. 658–664, 2008.

[2] M. Badr-el Dine, "Value of ear endoscopy in cholesteatoma surgery," *Otology & Neurotology*, vol. 23, no. 5, pp. 631–635, 2002.

[3] P. Golanó, J. Vega, L. Pérez-Carro, and V. Götzens, "Ankle anatomy for the arthroscopist. part I: The portals," *Foot and Ankle Clinics*, vol. 11, no. 2, pp. 253–273, 2006.

[4] H. B. Gilbert, D. C. Rucker, and R. J. Webster III, "Concentric tube robots: The state of the art and future directions," *International Symposium of Robotics Research*, 2013, To appear in *Springer Tracts on Advanced Robotics*.

[5] J. Burgner, D. Rucker, H. Gilbert, P. Swaney, P. Russell, K. Weaver, and R. J. Webster III, "A telerobotic system for transnasal surgery," *IEEE/ASME Transactions on Mechatronics*, vol. 19, no. 3, pp. 996–1006, June 2014.

[6] J. Burgner, P. J. Swaney, R. A. Lathrop, K. D. Weaver, and R. J. Webster III, "Debulking from within: a robotic steerable cannula for intracerebral hemorrhage evacuation," *IEEE Transactions on Biomedical Engineering*, vol. 60, no. 9, pp. 2567–2575, 2013.

[7] C. Bergeles and P. Dupont, "Planning stable paths for concentric tube robots," *IEEE/RSJ Internatinoal Conference on Intelligent Robots and Systems*, pp. 3077–3082, 2013.

[8] C. Bedell, J. Lock, A. Gosline, and P. Dupont, "Design optimization of concentric tube robots based on task and anatomical constraints," *IEEE International Conference on Robotics and Automation*, pp. 398–403, May 2011.

[9] K. Harada, K. Tsubouchi, M. Fujie, and T. Chiba, "Micro manipulators for intrauterine fetal surgery in an open MRI," *IEEE International Conference on Robotics and Automation*, pp. 502–507, 2005.

[10] P. Berkelman and J. Ma, "A compact modular teleoperated robotic system for laparoscopic surgery," *International Journal of Robotics Research*, vol. 28, no. 9, pp. 1198–1215, 2009.

[11] J. Shang, D. Noonan, C. Payne, J. Clark, M. H. Sodergren, A. Darzi, and G. Yang, "An articulated universal joint based flexible access robot for minimally invasive surgery," *IEEE International Conference on Robotics and Automation*, pp. 1147–1152, 2011.

[12] A. J. Madhani and J. K. Salisbury, "Wrist mechanism for surgical instrument for performing minimally invasive surgery with enhanced dexterity and sensitivity," Aug. 25 1998, US Patent 5,797,900.

[13] W.-H. Shin and D.-S. Kwon, "Surgical robot system for single-port surgery with novel joint mechanism," *IEEE Transactions on Biomedical Engineering*, vol. 60, no. 4, pp. 937–944, April 2013.

[14] B. Zhao and C. A. Nelson, "Decoupled cable-driven grasper design based on planetary gear theory," *Journal of Medical Devices*, vol. 7, no. 2, p. 020918, 2013.

[15] F. Jelínek, R. Pessers, and P. Breedveld, "Dragonflex–smart steerable laparoscopic instrument," *Journal of Medical Devices*, vol. 7, no. 2, p. 020911, 2013.

[16] C. Ishii and K. Kobayashi, "Development of a new bending mechanism and its application to robotic forceps manipulator," *IEEE International Conference on Robotics and Automation*, pp. 238–243, 2007.

[17] F. Hammond, R. Howe, and R. Wood, "Dexterous high-precision robotic wrist for micromanipulation," *International Conference on Advanced Robotics*, pp. 1–8, Nov 2013.

[18] M. B. Hong and Y.-H. Jo, "Design of a novel 4-dof wrist-type surgical instrument with enhanced rigidity and dexterity," *IEEE/ASME Transactions on Mechatronics*, vol. 19, no. 2, pp. 500–511, April 2014.

[19] D. P. Losey, P. A. York, P. J. Swaney, J. Burgner, and R. J. Webster III, "A flexure-based wrist for needle-sized surgical robots," *SPIE Medical Imaging*, pp. 86 711G–86 711G, 2013.

[20] J. Arata, Y. Saito, and H. Fujimoto, "Outer shell type 2 dof bending manipulator using spring-link mechanism for medical applications," *IEEE International Conference on Robotics and Automation*, pp. 1041–1046, 2010.

[21] W. Sieklicki, M. Zoppi, and R. Molfino, "Superelastic compliant mechanisms for needlescopic surgical wrists," *ASME/IFToMM International Conference on Reconfigurable Mechanisms and Robots*, pp. 392–399, 2009.

[22] P. Breedveld, "Steerable laparoscopic cable-ring forceps," *Journal of Medical Devices*, vol. 4, p. 027518, 2010.

[23] T. Y. Nai, J. L. Herder, and G. J. Tuijthof, "Steerable mechanical joint for high load transmission in minimally invasive instruments," *Journal of Medical Devices*, vol. 5, no. 3, 2011.

[24] J. Peirs, H. Van Brussel, D. Reynaerts, and G. De Gersem, "A flexible distal tip with two degrees of freedom for enhanced dexterity in endoscopic robot surgery," *Proceedings of the 13th Micromechanics Europe Workshop*, pp. 271–274, 2002.

[25] N. Simaan, "Snake-like units using flexible backbones and actuation redundancy for enhanced miniaturization," *IEEE International Conference on Robotics and Automation, 2005*, pp. 3012–3017, 2005.

[26] H. Fischer, B. Vogel, W. Pfleging, and H. Besser, "Flexible distal tip made of nitinol (NiTi) for a steerable endoscopic camera system," *Materials Science and Engineering: A*, vol. 273, pp. 780–783, 1999.

[27] M. D. M. Kutzer, S. M. Segreti, C. Y. Brown, M. Armand, R. H. Taylor, and S. C. Mears, "Design of a new cable-driven manipulator with a large open lumen: Preliminary applications in the minimally-invasive removal of osteolysis," *IEEE International Conference on Robotics and Automation*, pp. 2913–2920, 2011.

[28] D. Wei, Y. Wenlong, H. Dawei, and D. Zhijiang, "Modeling of flexible arm with triangular notches for applications in single port access abdominal surgery," *IEEE International Conference on Robotics and Biomimetics*, pp. 588–593, Dec 2012.

[29] J. Liu, B. Hall, M. Frecker, and E. W. Reutzel, "Compliant articulation structure using superelastic nitinol," *Smart Materials and Structures*, vol. 22, no. 9, p. 094018, 2013.

[30] J.-S. Kim, D.-Y. Lee, K. Kim, S. Kang, and K.-J. Cho, "Toward a solution to the snapping problem in a concentric-tube continuum robot: Grooved tubes with anisotropy," *IEEE International Conference on Robotics and Automation*, pp. 5871–5876, 2014.

[31] H. Azimian, P. Francis, T. Looi, and J. Drake, "Structurally-redesigned concentric-tube manipulators with improved stability," *IEEE/RSJ International Conference on Intelligent Robots and Systems*, pp. 2030–2035, 2014.

[32] Y. Haga, Y. Muyari, S. Goto, T. Matsunaga, and M. Esashi, "Development of minimally invasive medical tools using laser processing on cylindrical substrates," *Electrical Engineering in Japan*, vol. 176, no. 1, pp. 65–74, 2011.

[33] J. A. Bell, C. E. Saikus, K. Ratnayaka, V. Wu, M. Sonmez, A. Z. Faranesh, J. H. Colyer, R. J. Lederman, and O. Kocaturk, "A deflectable guiding catheter for real-time mri-guided interventions," *Journal of Magnetic Resonance Imaging*, vol. 35, no. 4, pp. 908–915, 2012.

[34] S. C. Ryu, P. Renaud, R. J. Black, B. L. Daniel, and M. R. Cutkosky, "Feasibility study of an optically actuated mr-compatible active needle," *IEEE/RSJ International Conference on Intelligent Robots and Systems*, pp. 2564–2569, 2011.

[35] R. J. Webster III and B. A. Jones, "Design and kinematic modeling of constant curvature continuum robots: a review," *The International Journal of Robotics Research*, vol. 29, no. 13, pp. 1661–1683, 2010.

[36] A. Pelton, J. DiCello, and S. Miyazaki, "Optimisation of processing and properties of medical grade nitinol wire," *Minimally Invasive Therapies and Allied Technologies*, vol. 9, pp. 107–118, 2000.

[37] R. Watkins and J. Shaw, "Shape memory alloy column buckling: An experimental study," *ICAST, Palm Beach, Aruba*, 2013.